JT-60U HIGH PERFORMANCE REGIMES

S. ISHIDA and THE JT-60 TEAM[1]
Japan Atomic Energy Research Institute,
Naka Fusion Research Establishment,
Naka-machi, Naka-gun, Ibaraki-ken,
Japan

Abstract

JT-60U HIGH PERFORMANCE REGIMES.

High performance regimes of JT-60U plasmas are presented with an emphasis upon the results from the use of a semi-closed pumped divertor with W-shaped geometry. Plasma performance in transient and quasi steady states has been significantly improved in reversed shear and high- β_p regimes. The reversed shear regime elevated an equivalent Q_{DT}^{eq} transiently up to 1.25 ($n_D(0)\tau_E T_i(0)=8.6\times10^{20}$ m-3•s•keV) in a reactor-relevant thermonuclear dominant regime. Long sustainment of enhanced confinement with internal transport barriers (ITBs) with a fully non-inductive current drive in a reversed shear discharge was successfully demonstrated with LH wave injection. Performance sustainment has been extended in the high- β_p regime with a high triangularity achieving a long sustainment of plasma conditions equivalent to $Q_{DT}^{eq}\sim0.16$ ($n_D(0)\tau_E T_i(0)\sim1.4\times10^{20}$ m^{-3}•s• keV) for ~4.5 s with a large non-inductive current drive fraction of 60-70% of the plasma current. Thermal and particle transport analyses show significant reduction of thermal and particle diffusivities around ITB resulting in a strong Er shear in the ITB region. The W-shaped divertor is effective for He ash exhaust demonstrating steady exhaust capability of τ_{He}^*/τ_E ~3-10 in support of ITER. Suppression of neutral back flow and chemical sputtering effect have been observed while MARFE onset density is rather decreased. Negative-ion based neutral beam injection (N-NBI) experiments have created a clear H-mode transition. Enhanced ionization cross-section due to multi-step ionization processes was confirmed as theoretically predicted. A current density profile driven by N-NBI is measured in a good agreement with theoretical prediction. N-NBI induced TAE modes characterized as persistent and bursting oscillations have been observed from a low hot beta of $<\beta_h>\sim0.1$-0.2% without a significant loss of fast ions.

1. INTRODUCTION

Since the operation started in 1991, JT-60U has addressed physics issues for reactor plasmas including ITER physics R&D and exploited new plasma regimes leading to a commercially attractive reactor such as SSTR in which highly confined plasmas are produced approaching a fusion reactor regime. JT-60U has taken the initiative in promoting experiments for steady state operation in two principal aspects of plasma performance and sustainment (eventually to steady state), in which it has increasingly become crucial to realize conditions relevant to those required for reactor plasmas self-consistently. To further this task, the N-NBI was for the first time introduced in 1996 and the reactor-relevant divertor modification was completed in 1997. JT-60U is now entering a new experimental phase for the self-consistent integration of individual performance.

This paper overviews the progress of JT-60U after the 1996 IAEA conference in view of performance in confinement, divertor and current drive needed for reactor plasmas, in which the best performances achieved during the last two years in JT-60U and physics understanding of the plasmas are presented. The results from the use of the newly installed divertor configuration are highlighted and discussed.

The modification from an open divertor to the W-shape divertor was completed in a shutdown period from February to May in 1997, and experiments with the modified divertor started in June 1997. As shown in Fig.1, this divertor configuration is characterized by a semi-closed divertor with a central dome, inner and outer divertor target plates, and a pumping slot for pump out from the private flux region, similar to the divertor for ITER. Reduction of chemical sputtering effect, back flow of neutral particles, heat load on the target tiles and impurities was expected from its design [1]. Target CFC tiles covering the divertor surfaces and the dome top were tapered to mitigate the concentration of heat load on the corner of tiles. Divertor pumping is done from a 3 cm gap of the inner slot through three perpendicular NBI ports using their cryopumps, where the effective pumping speed for deuterium at the pumping slot was measured to be typically ~13 m^3/s. As a consequence, available number of positive-ion based neutral beam injection (P-NBI) units are reduced from 14 units to 11 units where cryopumps for the three perpendicular beam units are dedicated for the use of divertor pumping. The divertor structure was designed to allow discharge operation up to 3 MA with a full field of 4.0 T at the vessel center. Boronization on the first wall using decaborane vapor has been regularly carried out in July 1997 and February 1998 after the divertor modification.

1 See Appendix.

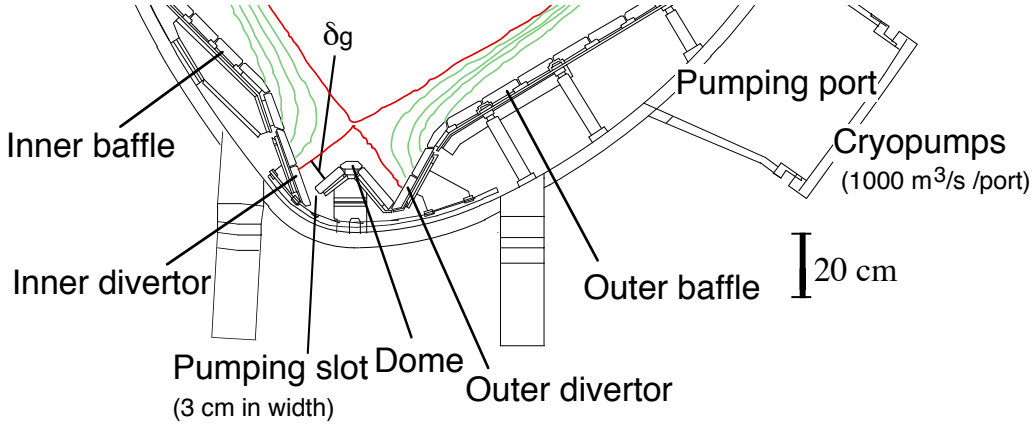

FIG.1. Poloidal cross section of the W-shaped divertor in JT-60U, showing a semi-closed pumped divertor with W-shaped geometry.

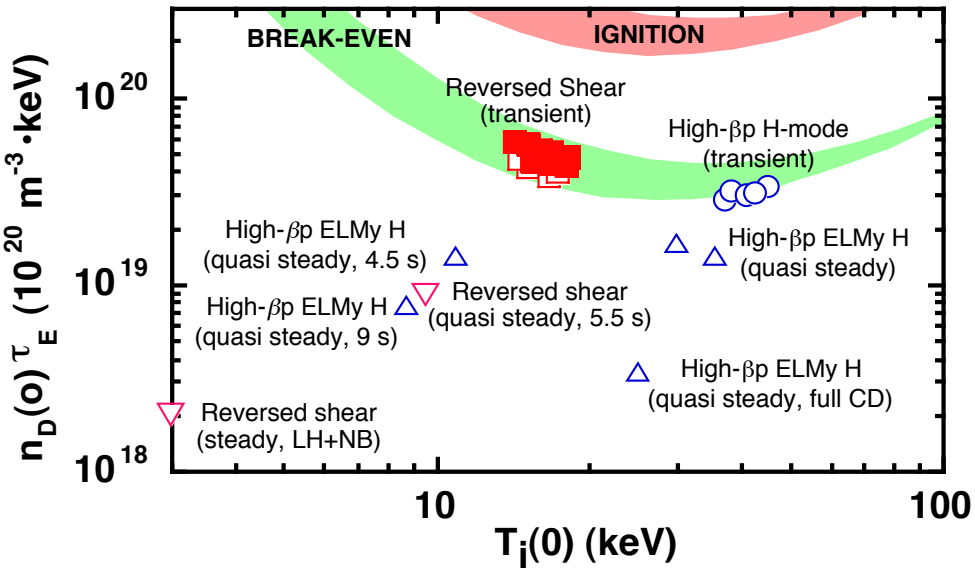

FIG. 2. Lawson diagram showing the parameters achieved in JT-60U where the discharges indicated in italic were achieved from Oct. 1996 to Oct. 1998.The closed symbol shows the discharge achieving $Q_{DT}^{eq}>1$.

2. HIGH PERFORMANCE REGIMES FOR STEADY STATE OPERATION

2.1 Two Approaches towards Steady State Operation of Tokamak Reactors

In JT-60U, two approaches of reversed shear and high-βp regimes have been attempted in different operational schemes to establish the prospects for steady state operation of tokamak reactors. The reversed shear regime with a negative central magnetic shear is widely considered attractive for a steady state operation with a large bootstrap current fraction in tokamak reactors since proposed for SSTR [2], as it would be possible to match the hollow current profile to a bootstrap current profile in a steady state. The high-βp regime produced in a monotonic q profile with central q above unity, which was developed in advance [3], can be also consistent with the steady state operation scenario under a substantial central current drive scheme as originally considered for SSTR [4].

TABLE I. ACHIEVED PARAMETERS IN JT-60U

Shot	E27969[8]	E31872[12]	E32611[12]	E29941[19]	E30006[19]
Mode	Reversed shear L-mode edge	Reversed shear L-mode edge	Reversed shear ELMy	High-βp H-mode ELMy	High-βp H-mode ELMy
Divertor	Open	W-shape	W-shape	W-shape	W-shape
time (s)	7.315	6.944	7.712	10.0	5.1
I_p (MA)	2.79	2.61	1.50	1.50	1.50
B_t (T)	4.34	4.37	3.50	3.72	3.63
P_{NB}^{abs} (MW)	16.0	11.77	9.54	22.1	15.0
a (m)	0.70	0.69	0.84	0.758	0.808
R_p (m)	3.10	3.08	3.31	3.30	3.25
δ	0.065	0.04	0.26	0.16	0.296
κ	1.97	1.92	1.49	1.58	1.56
q_{95}	3.15	3.17	4.31	3.99	4.46
W_{dia} (MJ)	10.9	8.17	3.29	3.86	4.73
dW_{dia}/dt (MW)	6.08	5.18	0.59	0	0
S_n (10^{16} /s)	4.52	3.63	0.427	0.851	1.04
Z_{eff}	3.49	3.19	3.23	2.0	2.3
$n_e(0)$ ($10^{19}m^{-3}$)	9.7	8.5	4.54	5.1	6.05
$n_D(0)$ ($10^{19}m^{-3}$)	4.9	4.8	2.51	4.09	4.48
$T_i(0)$ (keV)	16.5	16.8	9.6	8.8	11
$T_e(0)$ (keV)	8.4	7.2	5.9	4.2	6.0
τ_E (s)	0.97	1.07	0.35	0.175	0.315
$H_{ITER89P}$	3.23	3.21	2.02	1.61	2.33
β_N	1.88	1.53	1.38	1.68	1.98
β_p	1.15	0.98	1.04	1.28	1.55
β_t (%)	1.66	1.32	0.70	0.88	1.0
$n_D(0)\tau_E T_i(0)$ (10^{20} m-3•s•keV)	7.80	8.59	0.84	0.58	1.55
Q_{DD} (10^{-3})	4.7	5.6	0.53	0.451	0.81
Q_{DT}^{eq}	1.05	1.25	0.12	0.11	0.177

The plasmas performance in JT-60U achieved in the two regimes is plotted in the Lawson diagram as shown in Fig.2 where the data reported in the previous IAEA meetings are included [5, 6]. The closed symbol indicates the discharge with $Q_{DT}^{eq}>1$ where Q_{DT}^{eq} is the equivalent fusion multiplication factor defined for transient conditions involving the dW/dt term in an assumed deuterium-tritium fuel of a 50:50 mixture using deuterium beams with the experimental beam energy [7]. The best performances in the regimes have been produced in a transient state (dW/dt>0) at higher currents. As performances in a quasi steady state (dW/dt~0) have been so far achieved at lower currents, progressive improvement in quasi steady performance would be possible with optimization at higher current; in this paper, "quasi steady" and "steady" denotes sustainment beyond the energy confinement time and the current diffusion time scales, respectively. Typical discharges for these regimes are discussed in the following subsections with main parameters in TABLE I.

2.2 Reversed Shear Regime

2.2.1 Fusion Performance

After the IAEA meeting in 1996, a dedicated campaign to improve the fusion performance of reversed shear discharges has been conducted with increasing the plasma current up to 3 MA. As a consequence, the achievement of a critical condition of Q_{DT}^{eq} in excess of unity has been accomplished for the first time in the reversed shear discharges in October 1996 [8]; Shot E27969 was the best with $Q_{DT}^{eq}=1.05$ at $I_p=2.8$ MA. The progress in fusion performance can be attributed to stable increase in the Ip maintaining a vast reversed shear region extended up to r/a~0.7-0.8 and controlling the beam deposition profile during the current ramp-up. Since the discharges tended to be unstable when the qmin crossed ~3, pre-programed beam power reduction was applied at that timing. During this phase, MHD modes localized near the ITB were observed similar to observation of a barrier localized mode in a high-β_p mode plasma in JT-60U [9] and in an enhanced reversed shear plasma in TFTR [10].

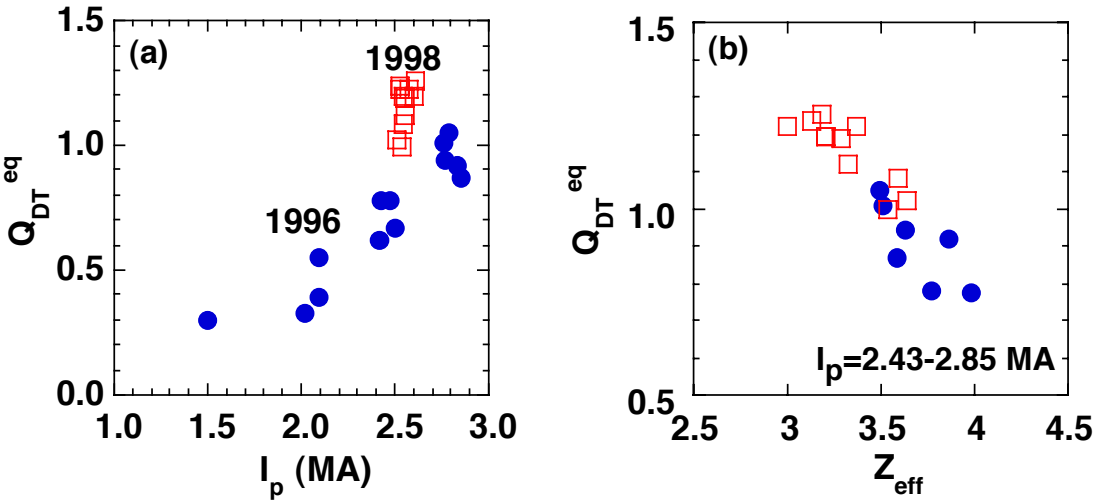

FIG. 3. Equivalent fusion multiplication factor (Q_{DT}^{eq}) as a function of (a) the plasma current and (b) Z_{eff} for high performance reversed shear discharges .

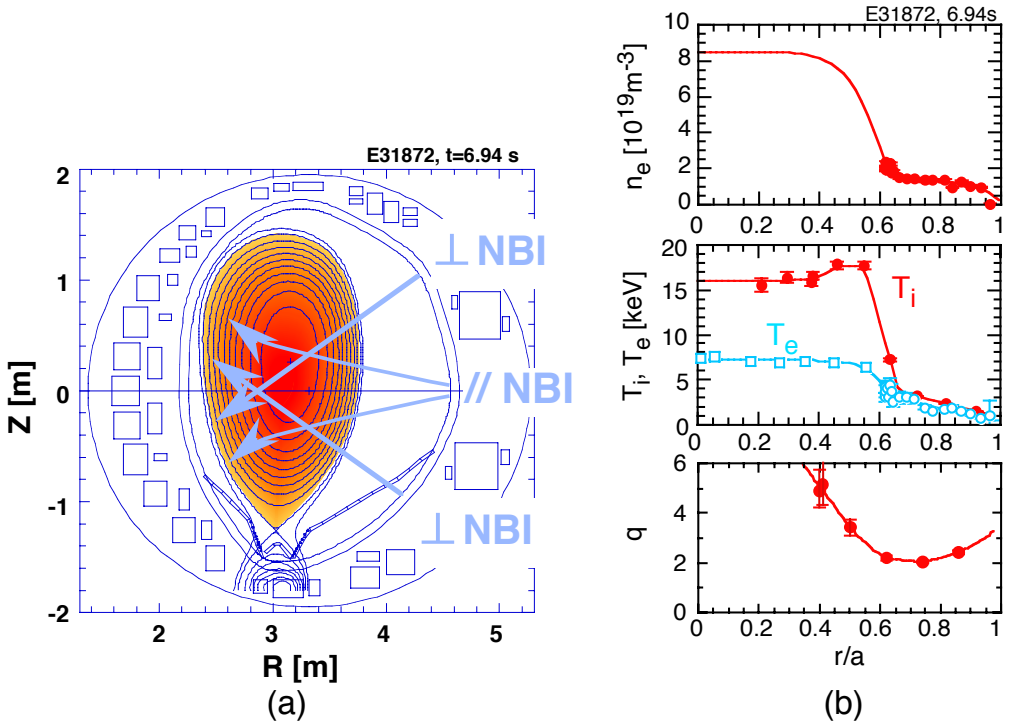

FIG.4. (a) An equilibrium configuration recontracted using motional stark effect (MSE) data for the discharge achieving Q_{DT}^{eq}=1.25 along with the injection paths of neutral beams, (b) the measured profiles of ion and electron temperature, electron density and the q profile at the same time.

Further improvement in the fusion performance was intensively attempted with the W-shaped divertor in 1998. Based on the operational scheme developed in the above campaign, the discharge optimization for the high performance reversed shear discharges has progressed utilizing feedback control of neutron emission rate by neutral beam injection power when the qmin crosses ~3. As the achieved Q_{DT}^{eq} values in the reversed shear regime are shown as a function of Ip in Fig.3(a), the Q_{DT}^{eq} value has been enhanced up to 1.25 at a lower current of 2.6 MA (Shot E31872) [11]. An equilibrium configuration aligned to the W-shaped divertor is shown in Fig.4 with the measured profiles at the time of peak performance for E31872. As shown in Fig.3, the Q_{DT}^{eq} value is increased with the plasma current. The improvement in fusion performance after the divertor modification is mainly attributed to a decrease in Z_{eff} as shown in Fig.3(b) and TABLE I [12]; the Z_{eff} value is inferred from matching the kinetic analysis of the neutron emission to the measured value assuming carbon as a dominant impurity.

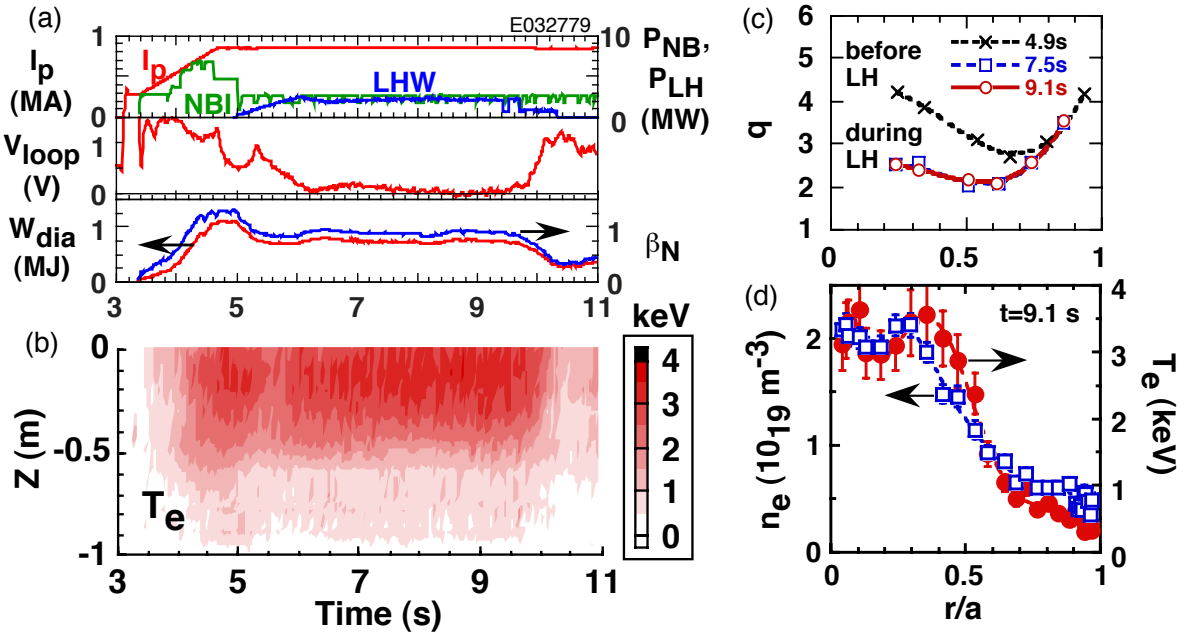

FIG.5. (a) Waveforms of a reversed shear discharge (I_p=0.85 MA, B_t=3.5 T) sustained with LH and NBI, (b) contour plots of the electron temperature profile evolution where the magnetic axis is placed at Z~+0.2 m above the midplane, (c) the q profiles at t=4.9 s, 7.5 s and 9.1 s, and (d) the electron density and ion temperature profiles at t=9.1 s for the same discharge.

The core plasma energy is efficiently confined due to the existence of persistent ITB formed for both ions and electrons at a large minor radius of r/a~0.7 near the boundary of the reversed shear region. The fusion performance of the reversed shear plasmas with an L-mode edge has been improved in a thermonuclear dominant regime relevant to reactor plasmas; where the thermal reaction fraction is calculated to be 82% for Shot E31872.

No high fusion performance discharges have been attained with qmin below ~2 in these campaigns. When the qmin closely approaches 2, the discharges tend to be disruptively terminated by a fast beta collapse at β_N~2 with the low q of q_{95}~3. At the β limit, ECE measurements with a fast sampling time of 5 μs actually show that the collapse develops from the ITB region and grows with a very fast time scale of the order of 10 μs [13]. From the ERATO-J code analysis, the observed β limits are found to be close to the ideal stability limits for low-n kink-ballooning modes [14].

2.2.2 ITB Sustainment

Quasi steady sustainment with NB: Quasi steady sustainment of the reversed shear mode confinement with a clear ITB has been achieved with an ELMy H-mode edge and an ITER-relevant triangularity shape of δ~0.3 by step down of beam injection power and combination of center and off-axis beams. In optimization of the pressure profile with the H-mode edge and triangular shaping, the operational beta limit close to an ideal beta limit was improved up to β_N~2.3 in a low qmin region down to q_{min}~1.5. A step down scheme for NBI to produce quasi steady reversed shear confinement with ITB has been established taking an operational margin for the beta limit. Enhanced confinement with $H_{ITER89P}$~1.7 and β_N~1.2 in the reversed shear discharges has been successfully sustained up to for 5.5 s (18 times τ_E) with a stored energy of ~3.0 MJ at I_p=1.5 MA and Bt=3.5 T for Shot E32611 (see TABLE I) [12].

Steady sustainment with NB and LH waves: The sustainment of the reversed shear discharge with enhanced confinement requires a current profile control scheme including non-inductive current drive externally applied consistently with a bootstrap current profile. LH (lower hybrid) current drive experiment in JT-60U addressed this issue demonstrating a long pulse reversed shear operation non-inductively sustained with enhanced confinement. As shown in Fig.5, the LH wave with power of ~2.3 MW was injected into a target reversed shear discharge with I_p=0.85 MA, B_t=2 T and P_{NB}=2.5 MW after the step down of the NB power. This discharge has achieved a fully non-inductive current drive with a bootstrap current fraction of ~23% to the total plasma current and a current drive efficiency of η_{CD}=1.3×10^{19} A/W/m^2 for the LHW-driven current [15]. An enhanced confinement with $H_{ITER89P}$≥

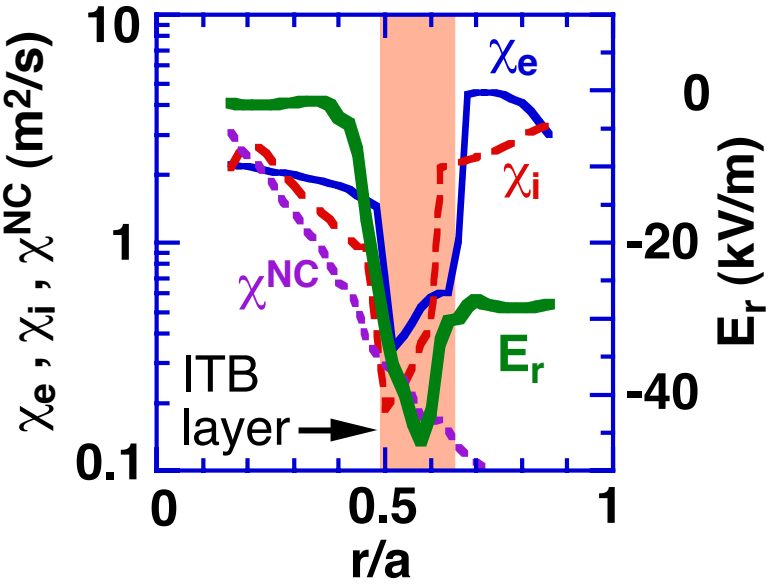

Fig. 6 Profiles of the ion and electron thermal diffusivities (χ_i and χ_e, respectively) and the radial electric field (E_r) in a reversed shear plasma with ITB along with the neoclassical diffusivity (χ_{NC}): I_p=1.5 MA and B_t=3.5T .

1.2 was sustained for ~ 6 s with clear ITBs observed for electron temperature and density profiles measured by a 14-channel YAG Thomson scattering system and the ion temperature profile until the LH power is turned-off. Until then, the reversed shear configuration is stationarily maintained in an excellent combination of the LH wave driven and bootstrap currents peaked at off-axis. This discharge has demonstrated that the enhanced confinement with ITB can be sustained with external current profile control as well as the plasma current, which may lead to a fusion power control scheme associated with ITB control in reactor plasmas.

2.2.3 Thermal Transport with ITB

The ITB plays an essential role in understanding the thermal transport in the reversed shear plasmas. Operational progress in sustaining the ITB longer than the energy confinement time for reversed shear discharges with ELMy H-mode edge, as discussed above, enables to study transport physics involving the ITB in a quasi steady state. In particular, the ITB observed in JT-60U has an outstanding feature that electron and ion thermal diffusivities are simultaneously reduced with a steep temperature gradient around a thin ITB layer [16]. To understand this plasma behavior, the radial electric field profile has been investigated in JT-60U in conjunction with a paradigm in which a sufficient ExB flow shear would suppress microinstabilities.

Transport analysis for the reversed shear discharges has been systematically carried out using a 1.5 dimension transport analysis code and an orbit following Monte-Carlo code. Figure 6 shows the ion and electron thermal diffusivities compared with the neoclassical diffusivity and the radial electric field for a reversed shear plasma (I_p=1.5 MA, B_t=3.5 T) with enhanced confinement associated with the presence of ITB. It is clearly shown here that, within a thin layer of ITB, the Er shear is drastically enhanced and both thermal diffusivities are significantly reduced to a neoclassical level.

Moreover, the FULL code analysis in collaboration with the PPPL group has shown that ExB shearing rate around an ITB region is as large as the linear growth rate of high-n toroidal drift mode for a reversed shear plasma [17]. The result suggests that a sheared ExB flow in the poloidal direction could suppress microinstabilities to generate the ITB for the reversed shear plasma in JT-60U.

2.2.3 Particle Transport with ITB

Particle confinement characteristics for reversed shear discharges were investigated in comparison with ELMy H-mode and high-β_p ELMy H-mode discharges with a particular emphasis on a separate treatment of particle sources between beam fueling and wall recycling/gas puffing [18]. An empirical scaling of the total number of fuel ions was obtained for the ELMy H-mode discharges in JT-60U. From comparison to this scaling, the particle confinement of the reversed shear discharge is found to be enhanced by more than a factor of two while that of the high-β_p ELMy H-mode discharges is not particularly enhanced.

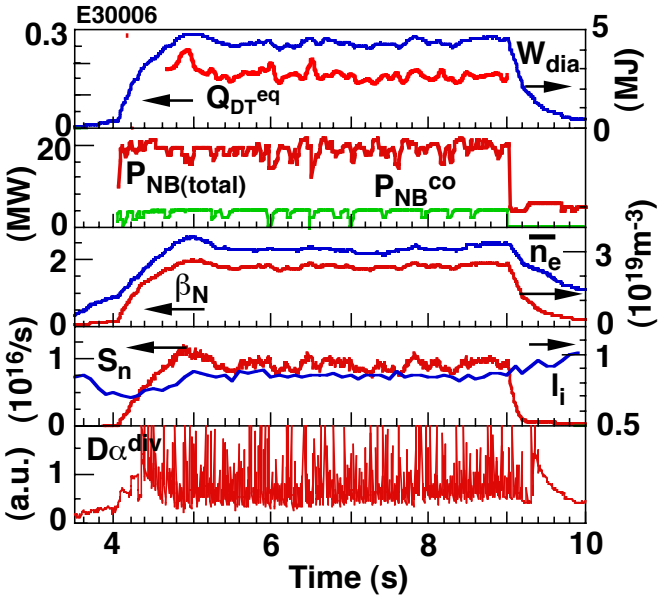

FIG. 7. Waveforms of a high performance high-β_p ELMy H-mode discharge sustained in a quasi steady state: I_p=1.5 MA and B_t=3.63 T.

The observed enhancement of the global particle confinement for the reversed shear discharges is closely related with the local particle transport involving the ITB. In terms of particle control for reactor plasmas, helium transport is crucially important for such a high particle confinement plasma as it is associated with a fuel dilution due to helium ash. To investigate the helium transport of the reversed shear plasma with enhanced confinement, the gas-puffing modulation experiment was performed as compared to that of the ELMy H-mode plasma [18]. From the results, the particle diffusivity of the reversed shear plasma is found to be significantly reduced within the ITB region indicating a dip in comparison with the ELMy H-mode case. Inward pinch velocity in the reversed shear plasma is evaluated to be broadly present similar to the ELMy H-mode plasma. This suggests that both beam and edge fuels can contribute to the enhancement of the global particle confinement of the reversed shear plasma discussed above.

2.3 High-β_p Regime

2.3.1 Improvement in Performance Sustainment

Simultaneous achievements of high confinement, high β limit, high bootstrap fraction and highly efficient exhaust of heat and particle in the divertor are required for steady state operation. The high-β_p regime has made significant progress in enhancing the sustainable performance with a high-β_p ELMy H-mode. Before the divertor modification, the duration of high performance period was limited by an increase in carbon impurities and deuterium recycling accompanied with a gradual decrease in energy confinement even though MHD activities would not appear.

After the divertor modification, deuterium recycling and carbon impurity influx have been remarkably reduced with the W-shaped divertor with pump, allowing a long pulse high power heating. The duration of high performance period was significantly extended for high-β_p ELMy H-mode. A high performance plasma with Q_{DT}^{eq}~0.11 successfully lasted for ~9 s (about fifty times energy confinement times) until the beams were switched off with $H_{ITER89P}$ ~1.7, $T_i(0)$~10 keV and β_N~1.8 under an intense beam injection power of 20-25 MW (see Shot E29941 in TABLE I). Although a total energy input reached 203 MJ (a record value in JT-60U), no increase in carbon impurity content and deuterium recycling was observed.

Increase in the triangular shaping of the plasma in the W-shaped divertor configuration has lead to enhancing the quasi-steady performance. As shown in Fig.7, a higher performance has been sustained at δ=0.3 with Q_{DT}^{eq}~0.16, $H_{ITER89P}$~2.3, β_N~2 and β_p~1.6 at I_p=1.5 MA and B_t=3.5 T for 4.5 s. Here, a large non-inductive current drive fraction of 60-70% of the plasma current is attained at a relatively high density of ~45% of the Greenwald limit. This performance was terminated due to a loss of the high δ equilibrium limited up to 5 s from a maximum heat capacity of the shaping coils. Performance sustainment in terms of Q_{DT}^{eq} value for the high-β_p ELMy H-mode discharges with the open and W-shaped divertor is summarized in Fig.8, showing that enhancement of the sustainment period has been realized with the high triangularity configuration possibly due to suppresion of recycling and carbon bursts in the use of the W-shaped divertor.

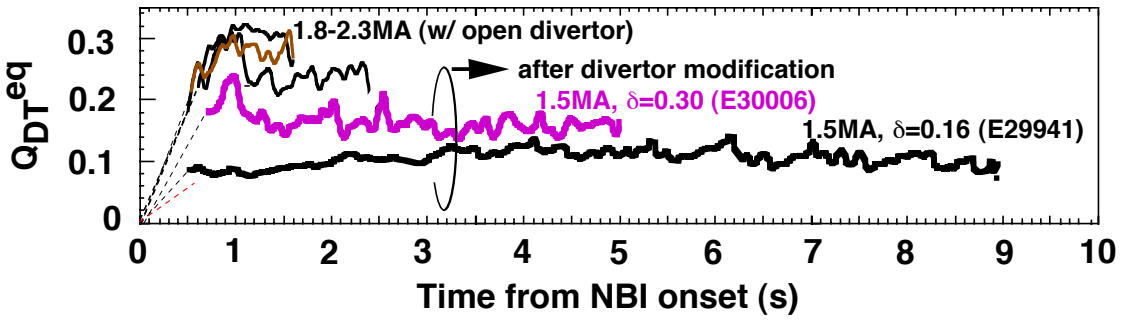

Fig. 8. Time traces of Q_{DT}^{eq} values for high-β_p ELMy H-mode discharges, where the discharges with the W-shaped divertor in comparison with the discharges with the open divertor.

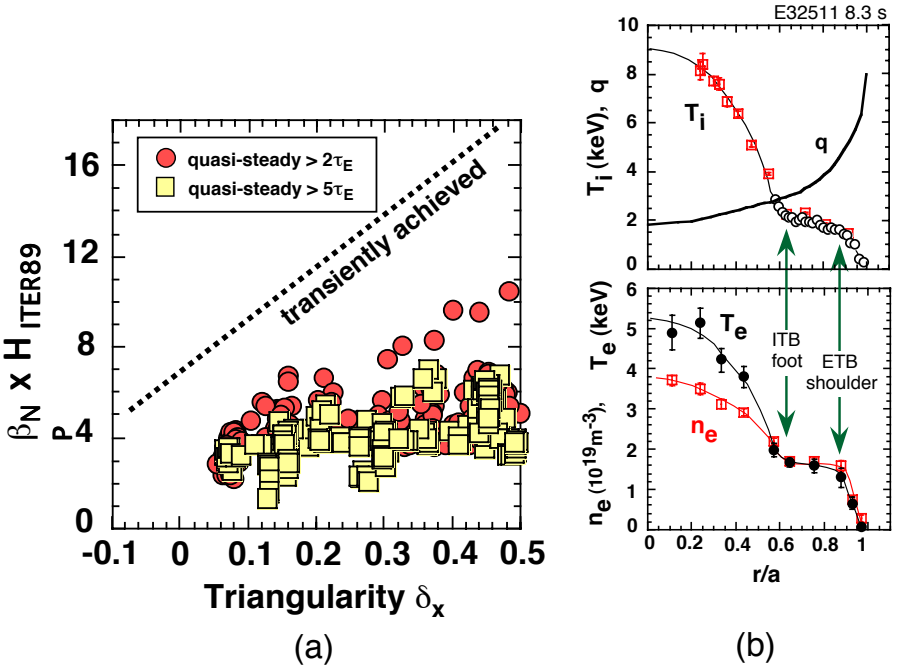

FIG. 9. (a) βNH values as a function of the triangularity in high-β_p regime for different sustainment durations along an upper envelop of the data achieved transiently, (b) profiles of the ion temperature, q profile, electron temperature and electron density showing internal and edge transport barriers for both ions and electrons in a high-β_p H-mode discharge;I_p=1 MA, B_t=3.6 T, δ=0.5, β_p=1.8, β_NH=3.5.

2.3.2 Sustainable Stability

Beta limits for long pulse high-β_p ELMy H-mode discharges appeared to be substantially lower than the ideal MHD limits. The appearance of low-n resistive modes has limited its sustainment, because sustainable β_N in a long pulse is lower (β_N~ 2 sustained for 5-9 s) than transiently achievable β_N (β_N~3.2 close to an ideal limit) due to these modes. Increase in the plasma triangularity and electron density should be beneficial for improving the long pulse stability [19]

As shown in Fig.9(a), the value of Hβ_N is found to increase with the triangularity in any duration from 'transient' to 'long pulse', while the level of Hβ_N decreases with extending sustainment time. Such a high triangular shaping is confirmed to be quite useful for improving the sustainable performance. Among discharges with dW/dt=0, Hβ_N decreases by ~40% from a short duration to quasi-steady>2s due to slowly growing resistive modes such as m/n=3/2, 2/1 and 3/1 with a time scale of the order of 100 ms. Suppression or control of these resistive modes could be another key to improve the sustainable performance.

With increasing triangularity, the features of internal and edge transport barriers appear to be changed. For a high-β_p H-mode discharge with δ=0.5 and β_p=1.8, a clear ITB for the electron temperature accompanied with ITBs for ion temperature and electron density was observed with

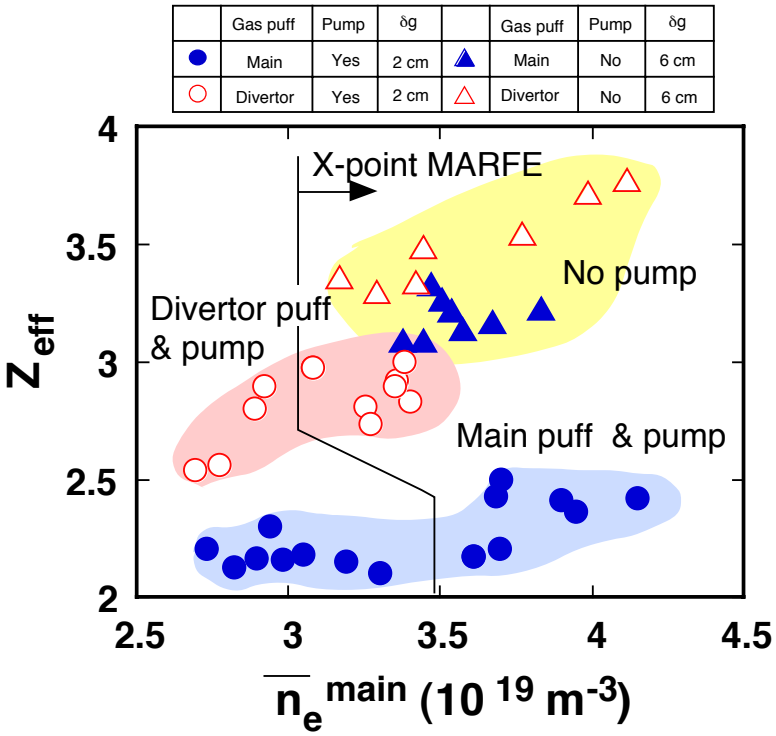

FIG. 10. Z_{eff} as a function of the line-averaged electron density showing effects of puff&pump and the gap width (δ_g) for ELMy H-mode discharges with I_p=1.2 MA and P_{NB}~18 MW.

an H-mode edge as shown in Fig. 9(b). This internal transport barrier is clearly located in a positive magnetic shear region for the non-reversed shear discharge. Recently, an ITB formation for electron temperature was observed in a positive shear region for a reversed shear discharge [20]. These observations may provide clues to understand physical mechanisms in the ITB formation and microturbulence suppression.

3. IMPROVED DIVERTOR PERFORMANCE

3.1 Effects of the Divertor Geometry

Effective gas puff and pump: After the divertor modification, carbon is the dominant impurity in JT-60U. The effects of a "gas puff and pump" scheme on reduction of Z_{eff} has been investigated for ELMy H-mode discharges with the W-shaped divertor configuration by changing the gap length (δ_g) between the pumping slot and the inner leg and by changing the location of gas puffing (main or divertor). Figure 10 shows that the gas puff and pump scheme with puffing from the main plasma region for the shorter gap length is the most effective in reducing the Z_{eff} value. This suggests that an enhanced SOL flow generated by the main gas puff and pump may contribute to the reduction of carbon impurities.

Reduction of neutral backflow: Suppression of back flow of neutral particles to the main plasma is a key role of the W-shaped divertor geometry. Substantial reduction of the neutral density at the main plasma and increase in the particle recycling in the divertor chamber were achieved in which the neutral ionization fluxes at the main plasma edge, $\Phi_{D\alpha}{}^{main}$, was reduced by a factor of 2-3 in comparison to the open divertor [21]. Thus, control efficiency of recycling neutrals is improved. Nevertheless, the threshold power for H-mode transition is not clearly reduced for the W-shaped divertor configuration [22].

Suppression of chemical sputtering effect: One of the important roles of this private dome is to reduce the generation of hydrocarbons due to chemical sputtering in the private region for suppression of MARFE onset at the X-point. To clarify the dome effect on carbon impurity reduction, profiles of CD band intensity have been investigated so that the CD-band intensity was clearly reduced in comparison with the open divertor case before the modification. The measured CD-band intensity profile was reproduced with IMPMC code using experimental data as shown in Fig.11.The result suggests that the dome works to prevent hydrocarbons invading upstream as predicted from the impurity transport code [23].

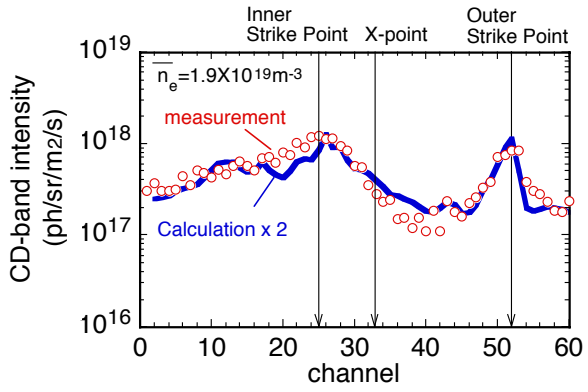

FIG. 11. Comparison of the profile of CD-band intensity from the divertor region between measurement and modelling calculation in the use of the W-shaped divertor.

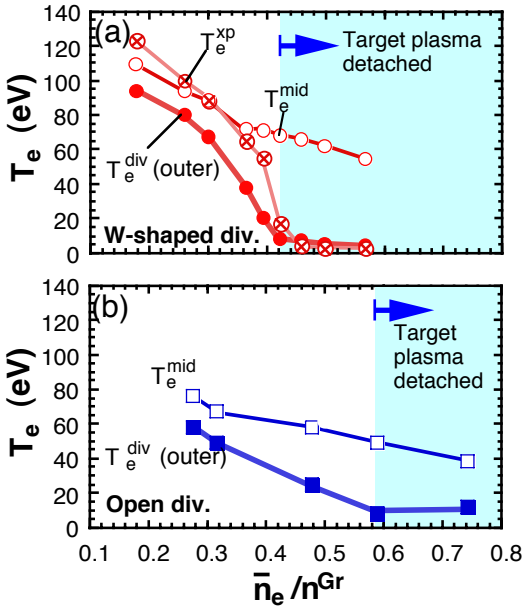

FIG. 12. Comparison of the electron temperature in SOL plasma at midplane, near x-point and at outer divertor target: (a) the W-shaped divertor and (b) the open divertor, along with density regions where MARFE is observed.

3.2 SOL Plasma Behavior

Detachment and MARFE: Detachment and MARFE onset density turn out to be ~20% lower in the W-shaped divertor than in the open divertor. Divertor and SOL plasma behaviors in terms of detachment process have been investigated for the W-shaped divertor using the Lanrmuir Mach probes installed at the midplane and the divertor X-point and the Langmuir probes at the target divertor plates [24]. Density dependence of the detachment formation for L-mode plasmas is shown in Fig.11 as compared with that in the open divertor where the electron temperature at the separatrix are more rapidly reduced with the electron density in the W-shaped. This may be caused by neutral particle condensation enhanced in the W-shaped divertor.

Reversal of SOL plasma flow: The SOL flow reversal has been observed for the case of the ion grad-B drift direction towards the divertor target and for ELMy H-modes, where the direction of the SOL plasma flow at the midplane is clearly revered though that just below the X-point orients the target. Quantitative evaluation of the drive mechanism: naturally produced in a torus to keep the pressure constant along the field line, was consistent with the measurement [24]. The SOL plasma flow may provide a clue to understand the present divertor plasma behaviors and should be important in reactor plasmas since He exhaust, impurity shielding and reduction in the main plasma recycling could be associated with the SOL plasma behavior.

3.3 Effective Divertor Pumping for He Ash Exhaust

In reactor plasmas, helium ash produced from DT fusion reactions should be continuously exhausted and controlled at a low level to sustain the controlled burning. In ITER, the ratio of effective helium pumping time to energy confinement time (τ_{He}^*/τ_E) is required to be below ~10 so that the helium density can be less than ~10% of the electron density. In JT-60U, the stationary helium exhaust capability has been investigated for ELMy H-mode and reversed shear discharges fully utilizing the divertor pumping from the inner private region with a large cryopump capability for helium exhaust in the use of an Argon frost method.

A necessary condition to purify the plasma for sustained self-ignition in ITER has been demonstrated in JT-60U during an ELMy H-mode with attached divertor condition [25]. As shown in Fig.13(a) energetic helium beams (E_b=60 keV, P_{NB}=1.4 MW) were injected into an ELMy H-mode discharge (I_p=1.4 MA, B_t=3.5 T, P_{NB}=12 MW) with $H_{ITER89P}$~1.3 for a duration sufficiently longer than the effective helium pumping time (τ_{He}^*~0.7 s) to simulate exhaust of helium ash

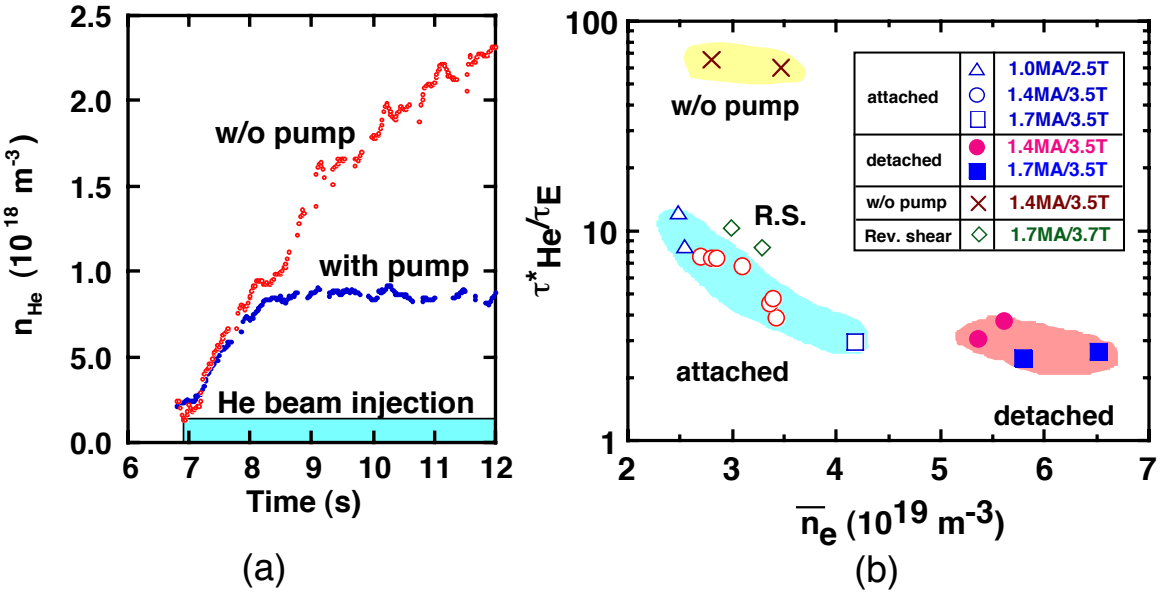

FIG. 13. (a) Temporal change of the helium density in the plasma in comparison between the cases with and without helium pumping during a long helium beam injection into an ELMy H-mode discharge, (b) the ratio of the effective helium pumping time to the energy confinement time as a function of the line-averaged electron density for ELMy H-mode discharges and reversed shear discharges.

produced in the central region of the plasma. The helium density was maintained at a low level (~4% of electron density) with $\tau_{He}^*/\tau_{E\sim4}$ in support of ITER. The helium enrichment factor (η) is evaluated to be 1.0 in excess of the required value of η=0.2 for ITER. These results are also confirmed by helium gas puffing experiments to simulate the thermalized and recycled helium ash in the peripheral region.

For the reversed shear discharges, however, the helium exhaust from the core plasma was found to be an issue since the particle confinement is enhanced in association with the ITB as discussed Section2.2.3. Helium exhaust experiments were carried out for the reversed shear discharges utilizing the helium gas puffing technique. The decay rate of the helium density at r/a=0.1 inside the ITB is found to be ~2 times longer than that at r/a=0.8 while the ITB is sustained, varying with the exhaust rate depending on the edge density. The helium exhaust is found to be even less effective since the helium outward flow is prevented due to the presence of ITB. This implies that it is necessary to consider the helium birth profile in a reactor plasma when the helium diffusivity is spatially altered due to the ITB.

The ratio of the effective He pumping time τ_{He}^* to the energy confinement time τ_E is summarized for ELMy H-mode discharges and reversed shear discharges as a function of the electron density in Fig.13(b) including the case of detached divertor and the case of no pump. It is clearly indicated that the present divertor pumping is capable of sufficiently exhausting helium ash even though the divertor plasma is detached for ELMy discharges.

3.4 Halo Currents

Halo current is generally observed as a current flow directly into a vacuum vessel from a plasma during disruptions in tokamaks. Since it can produce an intense electromagnetic force on the in-vessel components such as blanket and divertor, the experimental verification of the halo current behavior in a large tokamak device is urgently required for ITER. In JT-60U, sensors for the halo current (Rogowski coils) were newly installed in the divertor modification period, enabling the measurement of its toroidal and poloidal distributions.

The driving force of the halo current is considered to be an electric field generated by the temporal decrease in toroidal and poloidal magnetic fluxes in a plasma which are caused by the vertical shift rate ($-dZ_j/dt$) and the plasma current decay rate ($-dI_p/dt$). In this view, the halo current behavior should directly depend on electron temperature and impurity contents in the halo region determining the plasma resistivity.

It is found that 1) the product ($TPF \bullet I_h/I_{p0}$) of the toroidal peaking factor and the normalized

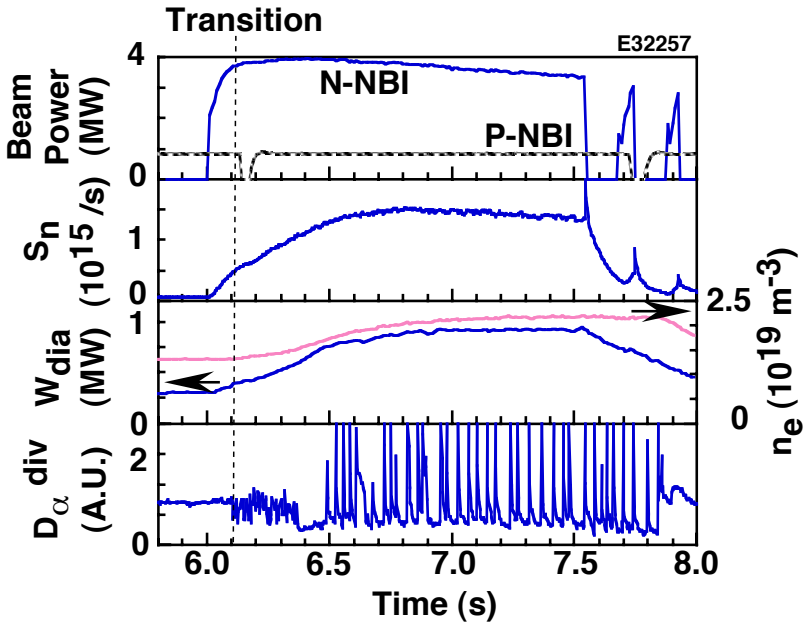

FIG. 14. Waveforms of N-NBI and P-NBI power, neutron emission rate, stored energy, electron density and D_α emissions from a divertor region, showing an H-mode transition induced by N-NB injection at a target electron density of $\overline{n}_e$~1.3×10^{19} m^{-3} for a discharge with I_p=1 MA and B_t=2.1 T.

halo current is lower than 0.52 and substantially below the maximum value of the ITER data base of 0. 75 where I_{p0} is the plasma current just before the current quench, 2) the halo current is lower for NB heated discharges corresponding to larger stored energy, and 3) neon gas puffing effectively reduces the halo current [26]. Parameter dependence of TPF•I_h/I_{p0} was systematically investigated in terms of electron density and stored energy. All these results provide a favorable view for future tokamaks that the halo current for high performance discharges could be smaller than for OH discharges and further reduction of the halo current could be obtained with intense neon gas puffing.

4. CURRENT DRIVE PERFORMANCE AND ENERGETIC PARTICLE EFFECTS

4.1 N-NB Current Drive

N-NBI commissioning: Since the N-NBI system was installed in JT-60U in 1996, the N-NBI commissioning has made progress in parallel with the use for experiments. The injection power has reached 5.15 MW for a pulse duration of 0.67 s at 350 keV. A new method termed 'pre-arcing', in which arc plasma is produced for 2 s in the ion sources prior to the beam extraction, allows the beam pulse duration to be extended up to 1.9 s with 3.37 MW at 357 keV for deuterium beams without breakdowns in electrodes. Consequently, the N-NBI triggered a clear H-mode transition as shown in Fig.14 [27]. Thus, N-NBI experiments have been performed to demonstrate the feasibility of current drive and heating by highly energetic beams necessary for reactor plasmas.

Multi-step ionization effects: It has a large impact on the determination of beam energy into reactor plasmas to verify whether the effective ionization cross-section of the beam in plasmas is enhanced by multi-step ionization processes as theoretically predicted. The N-NBI experiments in JT-6 0U have confirmed that the experimental enhancement agrees with the theoretical predictions from Janev et al. in the use of the N-NBI with 2.7-2.9 MW at 350 keV [28].

N-NB current drive: To exhibit the current drive capability of N-NBI, experiments aiming at N-NB current drive have been carried out with optimization of the target plasma with high electron temperature for improving the current drive efficiency. The profile of currents driven by the energetic beams from the N-NBI was identified from the MSE measurements in collaboration with the DIII-D group. The measured profile is in a good agreement of the theoretical prediction using the ACCOME code as shown in Fig.15: I_p=1.0 MA, B_t=3.5 T, $P_{N\text{-}NB}$=3.7 MW at 360 keV, $P_{P\text{-}NB}$=3.0 MW, n_e=0.87 $\times10^{19}$ m-3, $T_e(0)$=4.2 keV. From this experiment, the N-NBI has achieved a beam current drive efficiency of 0.6×1019 A/W/m^2 and a relatively large driven current of 0.6 MA [27]. Establishment of the evaluation scheme for the current drive performance with the energetic beams in JT-60U provide a definite view that current drive performance in fusion reactors is predictable, which is a significant contribution to ITER physics R&D.

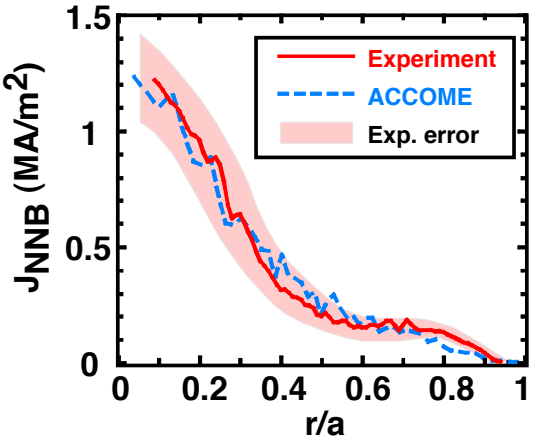

FIG. 15. Comparison of the N-NBI driven current density profile between measurement and ACCOME code calculation: I_p=1.0 MA, B_t=3.5 T and $P_{N\text{-}NB}$=3.7 MW.

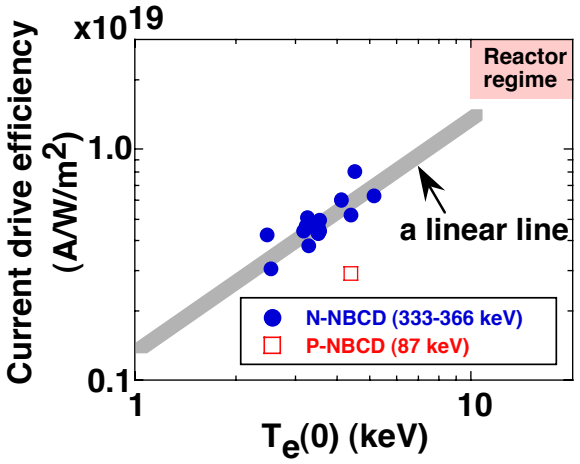

FIG. 16. Current drive efficiency of the N-NBI as a function of the central electron temperature in comparison with P-NBI.

Current drive efficiency: The current drive efficiency achieved for N-NBI are shown as a function of the central electron temperature in Fig.16 as compared with that for the P-NBI where the results are shown in the case of deuterium beams into deuterium plasmas. The current drive efficiency is found to be almost linearly increased with the temperature and improved with the beam energy [27]. This gives a prospect that N-NB injection into a high performance plasma with higher electron temperature above 10 keV would demonstrate a reactor-relevant current drive efficiency in JT-60U.

4.2 N-NB induced TAE Modes

A degradation of heating and current drive efficiencies due to excitation of a toroidicity-induced Alfvén eigen mode (TAE mode) is a major concern for the use of N-NBI. In JT-60U, N-NBI experiments have been performed in a low magnetic shear regime of q above unity or shear reversal to elucidate the TAE mode behavior during the injection of energetic beams. The N-NBI has the advantage for analysis that the deposition profile and velocity distribution are well known. The N-NBI is found to induce TAE modes observed as persistent and bursting oscillations. These modes were observed with low toroidal mode numbers from a significantly low hot beta (β_h) of $<\beta_h>$~0.1-0.2% [29]. In a diagram in terms of $<\beta_h>$ and $v_{b//}/v_A$ ($v_{b//}$: parallel velocity of beam ions, v_A: Alfvén velocity), the onset boundary for these TAE modes in JT-60U is found to be substantially below that for the burst-type TAE modes observed with tangential beam injection in TFTR [30] and DIII-D [31].

Persistent oscillations of TAE modes were observed with H^0-NNB injection (360 keV, 1.5-2 MW) into helium plasmas produced at 1.7 T during a ramp up phase of the plasma current resulting in a weak magnetic shear configuration as shown in Fig. 17. The TAE modes continue for 0.35 s and appears at $<\beta_h>$~0.09% and $v_{b//}/v_A$~0.4-0.7. The results from the NOVA-K code analysis assuming a q profile with q_0=1.4 are found to be consistent with the occurrence of the n=1 and 2 modes.

When the hot beta is increased, the persistent feature tends to become bursting with an observable degradation of the neutron emission rate. Burst modes with n=1 (40-70 kHz) and n=2 (70-110 kHz) were excited when D^0-NNB (350 keV, 2.6-3 MW) was injected into a deuterium plasma, where $v_{b//}/v_A$~0.5-0.6 and $<\beta_h>\geq$0.2%. The amplitude of magnetic fluctuations of the burst modes is about ten times as large as that of the persistent modes. A few % drops in the neutron emission rate is accompanied with the bursting activities. However, the present level of TAE modes in a range of up to $<\beta_h>$~0.6% do not result in a significant loss of co-injected N-NB ions.

5. CONCLUSIONS AND FUTURE DIRECTIONS

The JT-60U experiments have extensively explored the aspects of confinement, divertor and current drive performances. As a consequence, the present divertor modification in JT-60U has been successfully attributed to the enhancement of both attainable and sustainable performances in prospect of steady state operation of tokamak reactors.

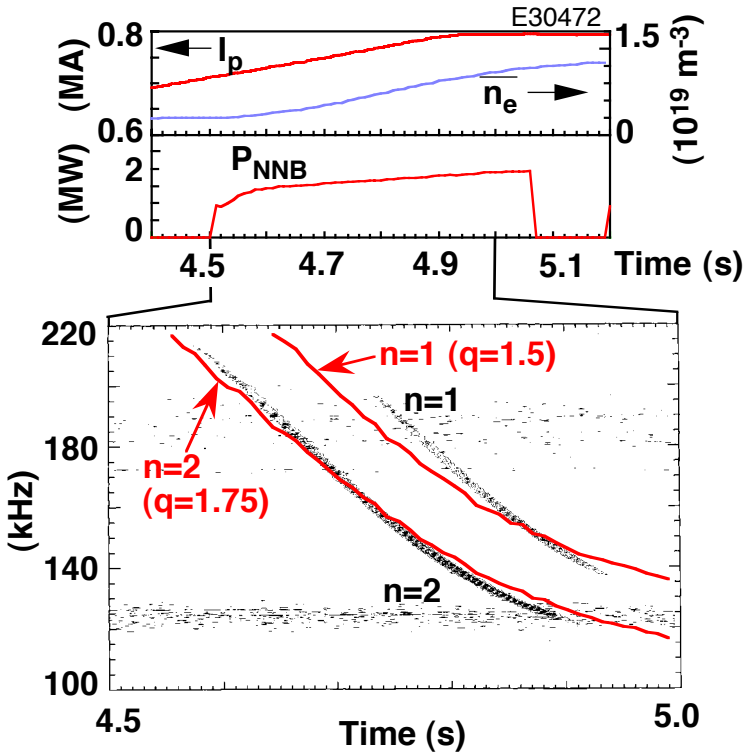

FIG. 17. Frequency spectrum of the NNB-induced TAE modes observed on the magnetic probe together with the waveforms of the discharge: B_t=1.7 T, where the frequencies for n=1 and n=2 modes evaluated for an assumed q profile are indicated.

The W-shaped divertor works to purify the plasma and suppress neutral back flow into the main chamber and hydrocarbons due to chemical sputtering in the private region. The divertor pumping is so effective that the He ash exhaust experiment demonstrates a steady exhaust capability in support of ITER. Thermal and particle transport studies have revealed the characteristic features of the plasma regimes elucidating causes and effects of the transport barriers.

In the use of the W-shaped divertor, the performance regimes have been significantly enhanced and extended as follows:

- Enhancement of the maximum performance in JT-60U has been attained in the reversed shear discharges up to Q_{DT}^{eq}=1.25 in a transient state,
- Sustainable performance and duration in a quasi steady state has been significantly improved in both reversed shear and high-β_p regimes with ELMy H-mode at the edge and the high triangularity shaping,
- A reversed shear discharge with ITB sustained by a full non-inductive current drive was demonstrated with LH wave injection combined with NBI.

The N-NBI has produced principal outcomes on the basis of which the extrapolation to a reactor regime would be assured, as the N-NBI experiments with up to 5.2 MW produce a clear H-mode transition, verify the theoretical predictability of currents driven by energetic beams and demonstrate the current drive efficiency increasing with electron temperature. TAE mode features induced by N-NBI start emerging uniquely in JT-60U, appearing from a significantly low hot beta without a significant loss of fast ions.

In the progress of the performance sustainment, a long pulse beta limit has become a crucial issue. To address this issue, the installation of an electron cyclotron heating (ECH) system with a few megawatts is planned to be installed in JT-60U where the ECH would be effective to suppress the resistive modes by controlling a local current profile. Moreover, as a minor modification for the W-shaped divertor, both side divertor pumping is planned by removing a shield masking the outer pumping slot to investigate the effects on SOL plasma flow, pumping capability and so on in comparison to the present inner slot pumping for optimization of the divertor concepts.

The JT-60U program is outstandingly progressed pursuing a reactor-grade plasma realized in a

steady state. The attempts planned in JT-60U will bring about a self-consistent integration of achieved performances under the maximum utilization of JT-60U facilities [32].

ACKNOWLEDGEMENTS

There have been continuous efforts of engineering and technical staffs in JT-60U and collaborative works with participants from universities, institutes and industries in Japan and foreign countries. Continued support and encouragement by Drs. M. Yoshikawa, H. Kishimoto and M. Ohta have enabled the present progress in the JT-60 programme.

REFERENCES

[1] N. Hosogane et al, Fusion Energy 1996 (Proc. 16th Int. Conf. Montreal, Canada 1996), IAEA, Vol.3, Vienna(1997)555.
[2] T. Ozeki et al. et al., Proceedings in Plasma Physics and Controlled Nuclear Fusion Research, Würzburg 1992 (International Atomic Energy Agency, Vienna), Vol.2, p.187, 1993.
[3] S. Ishida et al., Phys. Rev. Lett. 68(1992)1531.
[4] M. Kikuchi, Nucl. Fusion 30(1990)265.
[5] The JT-60 Team , Plasma Physics and Controlled Nuclear Fusion Research 1994 (Proc. 15th Int. Conf. Seville, 1994), IAEA, Vol.1, Vienna(1995)31.
[6] K. Ushigusa et al., Fusion Energy 1996 (Proc. 16th Int. Conf. Montreal, Canada 1996), IAEA, Vol.1, Vienna(1997)37.
[7] T. Fujita et al., Fusion Energy 1996 (Proc. 16th Int. Conf. Montreal, Canada 1996), IAEA, Vol.1, Vienna(1997)227.
[8] S. Ishida, et al., Phys. Rev. Lett., 79(1997)3917.
[9] S. Takeji et al., Phys. Plasmas 4 (1997)4283.
[10] J. Manickam et al., , IAEA-CN-69/EX8/4, this volume.
[11] K. Tobita, et al., to be published in Plasma Phys. Contro. Fusion.
[12] T. Fujita, et al., IAEA-CN-69/EX1/2, this volume.
[13] S. Ishida et al., et al., Proc. 24th European Conference on Controlled Fusion and Plasma Physics, Berchtesgaden, 1997, Part II-489.
[14] Y. Ishii et al., Plasma Phys. Contro. Fusion 40(1998)1607.
[15] S. Ide et al., IAEA-CN-69/CD1/4, this volume.
[16] T. Fujita et al., Phys. Rev. Lett. 78(1997)2377.
[17] H. Shirai et al, IAEA-CN-69/EX5/4, this volume.
[18] H. Takenaga et al., IAEA-CN-69/EXP1/17, this volume.
[19] Y. Kamada, et al., IAEA-CN-69/CD2/EX9/2, this volume.
[20] Y. Koide et al., IAEA-CN-69/EX5/2, this volume.
[21] N. Asakura et al., to be published in J. Nucl. Mater.
[22] K. Tsuchiya, Plasma Phys. Control. Fusion 40(1998)713.
[23] N. Hosogane et al., IAEA-CN-69/EXP4/05(R), this volume; K. Shimizu et al., J. Nucl. Mater. 241-243(1997)167.
[24] N. Asakura et al., IAEA-CN-69/EXP4/06(R), this volume.
[25] A. Sakasai et al., IAEA-CN-69/EX6/5, this volume.
[26] Y. Neyatani et at., IAEA-CN-69/EXP3/11, this volume.
[27] T. Oikawa et al., IAEA-CN-69/CD1/1, this volume.
[28] M. Nemoto et al., J. Plasma and Fusion Research 73(1997)1357.
[29] Y. Kusama et al., IAEA-CN-69/EX8/6, this volume.
[30] K.L. Wong et al., Pyhs. Rev. Lett. 66(1991)1874.
[31] E.J. Strait et al., Nucl. Fusion 33(1993)1849.
[32] K. Ushigusa et al., IAEA-CN-69/FTP/12.

Appendix

THE JT-60 TEAM

H. Adachi*), H. Akasaka, N. Akino, K. Annou, T. Arai, K. Arakawa, N. Asakura, M. Azumi, P.E. Bak[1)], C.Z. Cheng[2)], S. Chiba, O. Dacosta[4)], S.A. Dettrick[5)], N. Ebihara, C.B. Forest[6)], G.Y. Fu[2)], T. Fujii, T. Fujita, T. Fukuda, H. Fukuda*), A. Funahashi, H. Furukawa*), X. Gao[7)], L. Grisham[2)], K. Haga*), K. Hamamatsu, T. Hamano*), Y. Hasegawa*), T. Hatae, N. Hayashi[18)], S. Higashijima, K. Hill[2)], S. Hiranai, H. Hiratsuka, T. Hiroi*), M. Honda, A. Honda, N. Hosogane, L. Hu[7)], S. Hudson[8)], H. Ichige, S. Ide, Y. Ikeda, A. Inoue*), M. Isaka, A. Isayama, N. Isei, S.Ishida, Y. Ishii, K.Ishii*), T. Ishijima[9)], K. Itami, T. Itoh, T. Iwahashi*), M. Iwase[10)], S.C. Jardin[2)], E. Kajiyama*), Y. Kamada, A. Kaminaga, T. Kashiwabara*), M. Kawai, Y. Kawamata, Y. Kawano, M. Kazawa, M. Kikuchi, T. Kimura, V. Kiptily[11)], Y. Kishimoto, S. Kitamura, K. Kiyono, K. Kodama, Y. Koide, M. Koiwa*), S. Kokusen*), K. Komuro*), T. Kondou, S. Konoshima, J. Koog[10)], G.J. Kramer[12)], H. Kubo, A. Kumagai[9)], K. Kurihara, G. Kurita, M. Kuriyama, Y. Kusama, L.L. Lao[13)], A. Makhankov[17)], J. Manickam[2)], K. Masaki, H. Masui*), T. Matsuda, M. Matsukawa, T. Matsumoto, Y. Meng[7)], D.R. Mikkelsen[2)], Y.M. Miura, K. Miyachi, H. Miyata*), K. Miyata*), Y. Miyo, K. Mogaki, M. Mori, M. Morimoto*), A. Morioka, S. Moriyama, M. Nagami, K. Nagashima, A. Nagashima, S. Nagaya, O. Naito, Y. Nakamura, T. Nakano, R. Nazikian[2)], M. Nemoto, H. Nemoto*), S.V. Neudatchin[14)], Y. Neyatani, H. Ninomiya, T. Nishitani, H. Nobusaka*), T. Ohga, M. Ohsawa[18)], K. Ohshima*), A. Oikawa, T. Oikawa, M. Okabayashi[2)], T. Okabe, J. Okano, S. Omori, Y. Omori, K. Omori, T. Ooba*), H. Oohara, T. Oshima, T. Ozeki, A. Polevoi[14)], G. Rewoldt[2)], J.A. Romero[15)], M. Saidoh, N. Saitoh, A. Sakasai, S. Sakata, T. Sakuma*), S. Sakurai, T. Sasajima, N. Sasaki*), M. Sato, Y. Seimiya, M. Seki, H. Seki*), M. Shimada, K. Shimizu, M. Shimizu, M. Shimono, K. Shinohara, S. Shinozaki, H. Shirai, M. Shitomi, X. Song[16)], A. Sugawara*), T. Sugie, H. Sunaoshi, M. Suzuki*), S. Suzuki[10)], S. Takahashi*), S. Takano*), S. Takeji, H. Takenaga, T. Takizuka, H. Tamai, Y. Tanai*), F.V. Tchernychev[19)], T. Terakado, M. Terakado, K. Tobita, S. Tokuda, T. Totsuka, R. Toyokawa*), N. Toyoshima, K. Tsuchiya, T. Tshuda, T. Tsugita, Y. Tsukahara, K. Uehara, Y. Uramoto, K. Ushigusa, K. Usui, J. Yagyu, M. Yamagiwa, T. Yamamoto, H. Yamazaki*), K. Yokokura, H. Yoshida, R. Yoshino, J. Zhao[7)]

*) Staff on loan
1) STA Fellow, EU(Denmark)
2) PPPL, U.S.A.
3) JET Undertaking, E.U.
4) STA Fellow, Ecole Polytech. France
5) Australia N. U., Australia
6) Univ. of Wisconsin, U.S.A.
7) STA Scientist Exchange, ASIPP, China
8) STA Fellow, Australian N. U.
9) JAERI-Tukuba Univ. Doctor Cource
10) Post-Doctoral Fellow
11) Ioffe Institute, RF
12) STA Fellow, Netherlands
13) GA, U.S.A.
14) Kurchatov, RF
15) STA Fellow, EU(Spain)
16) STA Scientist Exchange, SWIP, China
17) D.V. Efremov Scientific Research Institute, RF
18) Fellow of Advanced Science
19) STA Fellow, Ioffe Institute, RF